

Many-body theory of false vacuum decay in quantum spin chains

Christian Johansen,^{1,*} Alessio Recati,^{1,2,†} Iacopo Carusotto,^{1,2,‡} and Alberto Biella^{1,2,§}

¹*Pitaevskii BEC Center, CNR-INO and Dipartimento di Fisica, Università di Trento, Trento, Italy*

²*INFN-TIFPA, Trento Institute for Fundamental Physics and Applications, I-38123 Trento, Italy*

(Dated: August 20, 2025)

In this work we theoretically investigate the false vacuum decay process in a ferromagnetic quantum spin-1/2 chain. We develop a many-body theory describing the nucleation and the coherent dynamics of true-vacuum bubbles that is analytically tractable and agrees with numerical matrix product state calculations in all parameter regimes up to intermediate times. This bosonic theory allows us to identify different regimes in the parameter space and unravel the underlying physical mechanisms. In particular, regimes that closely correspond to the cosmological false vacuum decay picture are highlighted and characterized in terms of observable quantities.

Metastability is a generic physical phenomenon where a system remains trapped in a long-lived excited configuration before transitioning to a stable lower-energy one under the effect of rare events triggered by either thermal or quantum fluctuations. Such metastable behaviors can be observed in a variety of quantum systems [1–3], from long-lived α -decaying nuclei [4, 5], to spatially extended condensed-matter systems undergoing a first-order phase transition in both the classical [6, 7] and quantum [8] regimes, and cosmological quantum field theories [9].

At low enough temperatures, escape from the metastable state generally requires a quantum tunneling process under the energetic barrier separating it from the true ground state. In spatially extended systems, the decay of the metastable state (the false vacuum – FV) generically occurs via the nucleation of ground state (true vacuum – TV) bubbles. In the latest years, such false vacuum decay (FVD) phenomena are receiving a renovated attention after recent experimental works in ultracold atomic condensates [10], quantum annealers [11], and cold-atom-based quantum simulators [12].

In this work, we will investigate FVD phenomena in the specific, yet paradigmatic case of a spin-1/2 chain undergoing a first-order ferromagnetic transition [13, 14]. Such configurations are experimentally realizable on various platforms, including real materials [15], well-controlled quantum simulators [16, 17] based on trapped ions [18], Rydberg atom in optical tweezers [19] and superconducting circuits [20]. As compared to the approximated techniques for cold atomic gases [21, 22] the simplicity of the spin-chain model allows for numerical simulations of the full quantum dynamics to be performed in a controlled way with matrix-product-state (MPS) techniques [23]. On the other hand, in spite of recent numerical investigations [8, 24], key questions on FVD phenomena are still open and ask for analytical developments. A theory for the early-time dynamics was put forward in [25] and related confinement and meson dynamics were explored in [26, 27]. Yet, the intermediate timescales where the actual FVD dynamics takes place has remained so far inaccessible to analytical treatment.

In this Letter, we present a comprehensive theoret-

ical study of the range of false vacuum decay effects that can be observed in spin-1/2 chains. We develop a novel theoretical approach to the real-time many-body dynamics following a quantum quench and we apply it to the bubble-nucleation process and the following bubble-expansion dynamics. Depending on the parameters, several regimes are identified, including one which closely recovers Coleman’s original picture of FVD in the cosmological context [28].

The physical system – We consider the quench dynamics of a spin-1/2 chain described by the Hamiltonian

$$H(t) = -J \left[\sum_{n=1}^{N-1} \sigma_n^x \sigma_{n+1}^x + \sum_{n=1}^N \left(h_{\perp} \sigma_n^z + \theta(t) h_{\parallel} \sigma_n^x \right) \right] \quad (1)$$

where σ_n^{α} are Pauli operators, h_{\perp} (h_{\parallel}) is the strength of the transverse (longitudinal) field, $J > 0$ sets the energy scale and the Heaviside function $\theta(t)$ describes the quench at $t = 0$. Throughout this work, we focus on the ferromagnetic phase $h_{\perp} < 1$ in the thermodynamic limit.

Before the quench, there is no longitudinal field. Among the two degenerate ground states with opposite magnetization $\langle \sigma_n^x \rangle = \pm M = \pm (1 - h_{\perp}^2)^{1/8}$, we assume that the system is initially prepared in the state of $+M$ magnetization, which we refer to as $|0^+\rangle$. Following the quench, the ground-state degeneracy is lifted by the finite longitudinal field h_{\parallel} ; specifically, our choice of $h_{\parallel} < 0$ renders $|0^+\rangle$ metastable.

Before the quench, the spin chain at zero longitudinal field is integrable and diagonalized by fermionic excitations [14, 29–31]

$$H(t < 0) = \int_{-\pi}^{\pi} \frac{d\theta}{2\pi} \epsilon(\theta) \gamma^{\dagger}(\theta) \gamma(\theta), \quad (2)$$

where $\gamma(\theta)$ annihilates a fermion at momentum θ and obeys the anti-commutation relations $\{\gamma(\theta), \gamma^{\dagger}(\theta')\} = 2\pi\delta(\theta - \theta')$. These fermionic excitations can be associated to smeared-out domain walls of width $W \approx \sqrt{h_{\perp}}/(1 - h_{\perp})$ [32]. Their dispersion relation $\epsilon(\theta) = 2J\sqrt{1 - 2h_{\perp}\cos(\theta) + h_{\perp}^2}$ displays a finite energy gap

$\epsilon(0) = 2J(1 - h_\perp)$ and a finite bandwidth $\Delta\epsilon = \epsilon(\pi) - \epsilon(0) = 4Jh_\perp$.

After the quench, the model becomes non-integrable, as the finite longitudinal field h_\parallel induces repulsive interactions between fermions of constant strength $\alpha = 2J|h_\parallel|M$ [33] and couples sectors that differ by an even number of fermions. In what follows, we will focus on the $\epsilon(0)/(J|h_\parallel|) \gg 1$ regime where the fermion creation/annihilation processes are weak and can be treated perturbatively in h_\parallel [34]. This is in contrast to the $\epsilon(0)/(Jh_\parallel) \ll 1$ regime where the strong, non-perturbative coupling between different fermion-number sectors prohibits the FVD phenomena from appearing.

A key element of the FVD process are the so-called bubbles of TV, separated from the surrounding FV by a pair of fermionic domain walls. To categorize the nature of the bubbles we introduce the bubble rigidity parameter $K \equiv \alpha/\Delta\epsilon$. As we are considering bubbles with vanishing total momentum the inverse rigidity $1/K$ quantifies the spatial expansion that bubbles can undergo as the interaction energy between fermions is transferred into their kinetic energy. When $K > 1$ only a small part of the interaction energy can be transferred into kinetic energy, so the bubble has a rigid character and maintains a well-defined size. In the opposite limit $K \ll 1$, the bubble is able to expand under the effect of the repulsive force between fermions. In the following we will consider parameter sets $p_{\rho,1/2}$ in the rigid bubble (RB) regime with $K \approx 4$ and parameter sets $p_{\chi,1/2}$ in the expandable bubble (XB) regime with $K \lesssim 0.04$.

Single-bubble theory – In both the rigid and the expandable regime one can first restrict to the two-fermion sector [25, 33]. Diagonalizing the corresponding two-body problem yields the energies E_L and the internal wavefunction $\phi_{L,n}$ of the L 'th zero-momentum two-fermion eigenstate, expressed as

$$|\phi_L\rangle = \frac{1}{\sqrt{2N}} \sum_{n,m} \phi_{L,n} b_{m+n}^\dagger b_m^\dagger |0^+\rangle, \quad (3)$$

in terms of the real-space fermionic annihilation operators $b_m = \int_{-\pi}^{\pi} d\theta e^{-i\theta m} \gamma(\theta)/2\pi$. Modulo the domain-wall smearing width W , each two-fermion term in the sum on the RHS of Eq. (3) describe a single TV bubble of size n . Thus, $|\phi_{L,n}|^2$ represents the weight of a TV bubble of size n in the L 'th single-bubble eigenstate.

The energies of the single-bubble eigenstates shown in Fig. 1.a result from the competition between the energy cost of creating two fermions (i.e., twice the gap) and the energy gained by forming a finite TV domain, associated to the linear repulsive interaction energy between fermions. A special attention goes to the resonant state, defined as the eigenstate $r = \arg \min_L |E_L|$ of energy E_r closest to zero energy. As the energy spacing is $\Delta E = 2J|h_\parallel|M$, good resonance $E_r \approx 0$ is naturally found for sufficiently small values of h_\parallel , as visible on

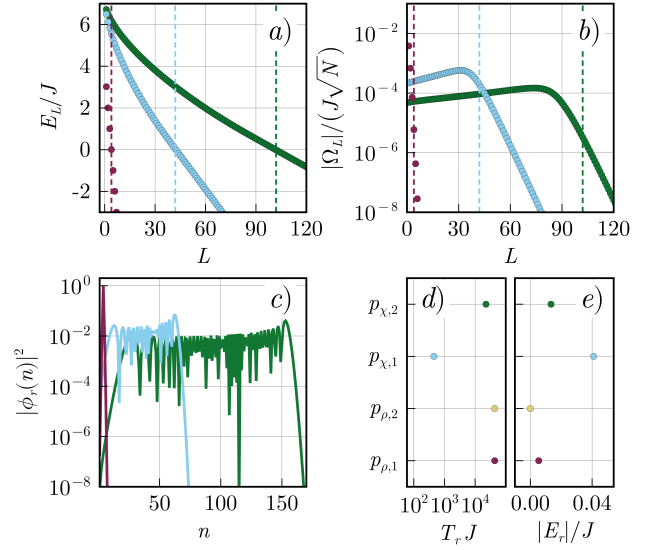


FIG. 1. Single-bubble eigenstates for four different parameter sets, labeled as $p_{\beta,n} = \{h_\perp, h_\parallel\}$. The two sets $p_{\chi,1} = \{0.75, 0.06\}$ and $p_{\chi,2} = \{0.75, 0.025\}$ are in the expandable bubble (XB) regime, while the two sets $p_{\rho,1} = \{0.06, 0.5\}$ and $p_{\rho,2} = \{0.06, 0.500675761\}$ are in the rigid bubble (RB) regime, the latter being fine-tuned to have a zero-energy resonant state. Panel a) shows the energies E_L of the single-bubble eigenstates; b) shows their coupling Ω_L to the initial false vacuum (FV) state $|0^+\rangle$, the resonant eigenstate being indicated by the vertical dashed lines. Panel c) shows the eigenfunction of the resonant eigenstate. Panels d) and e) give the associated timescale and the energy of the resonant eigenstate, and also serve as the color legend for all subplots. In panels a)-c), results for $p_{\rho,1/2}$ are indistinguishable.

$p_{\chi,1/2}$ in Fig. 1.a. However, also for relatively large h_\parallel , a fine-tuning of h_\parallel can be used to set $E_r \approx 0$ with no appreciable change in the other properties, as illustrated in $p_{\rho,2}$ in Fig. 1.e. Most importantly, the rigid vs. expandable nature of the bubbles is apparent in the structure of the eigenfunctions, e.g. in the resonant eigenfunctions shown in Fig. 1.c. In the RB regime, a single bubble size dominates each eigenstate and the wavefunction is strongly peaked around the classically expected resonant bubble size $l_r = 2(1 - h_\perp)/(|h_\parallel|M)$. In contrast, in the XB regime, many bubble sizes contribute significantly, rendering the eigenstate spatially delocalized also in the relative distance between the turning points at $l_r^\pm = 2(1 \pm h_\perp)/(|h_\parallel|M)$.

In order to describe the FVD dynamics, we need to determine the coupling $\Omega_L = \langle 0^+ | V | \phi_L \rangle$ between the initial FV state and each single-bubble eigenstates under the effect of the longitudinal field h_\parallel [25, 33, 35]. These couplings are plotted in Fig. 1.b and exhibit clear qualitative differences between the RB and XB regimes. Unlike E_r , the difference between these couplings are primarily controlled by h_\perp , as indicated by the relative difference

$$|(\Omega_{r-1} - \Omega_{r+1})/\Omega_r| \approx h_\perp^{-1} - h_\perp, \quad (4)$$

which goes to zero as $h_\perp \rightarrow 1$ in the XB regime, indicating the possibility of coupling also to large bubbles. Furthermore, in contrast to the fast exponential decay of the RB regime, in the XB regime Ω_L displays a plateau for the positive energy states, which results in a finite number of eigenstates having comparable coupling to $|0^+\rangle$. Interestingly, the timescale for the resonant processes $T_r = |\Omega_r|^{-1}$, plotted in Fig. 1.d, varies by nearly two orders of magnitude across the parameter sets, highlighting the generality of the physical mechanisms.

Based on the single-bubble excitations, one can describe short-time dynamics arising from creation and annihilation of single TV bubbles as discussed, e.g., in [25]: as long as the TV density remains negligible, this single-bubble theory is highly effective. However, it fails to capture the FVD process, which requires accounting for a finite density of TV domains. This is the goal of our coherent bubble theory.

Coherent bubble theory – As the generic many-body problem is exceedingly complex, we restrict our analysis to a dilute regime where the system has a small but finite density of bubbles so interactions between bubbles can be neglected. In what follows, we will see that this is enough to accurately describe the physics of the FVD process.

Based on the single-bubble eigenstates introduced above and on their coupling to the initial $|0^+\rangle$ state, we can construct a second-quantized theory in terms of bubble creation operators

$$d_L^\dagger = \frac{1}{\sqrt{2N}} \sum_{n,m=1}^N \phi_{L,n} b_{m+n}^\dagger b_m^\dagger. \quad (5)$$

Analogously to composite bosons such as bound electron-hole pairs in semiconductor materials, the so-called excitons [36–38], the bubble operators obey approximately bosonic commutation relations

$$[d_L, d_{L'}^\dagger] = \delta_{L,L'} - \frac{2}{N} \sum_{n,m,m'=1}^N \phi_{L,n}^* \phi_{L',m} b_{m-n+m'}^\dagger b_{m'}, \quad (6)$$

where the second term encodes corrections to the bosonic statistics arising from the underlying fermionic correlations. As these correction terms are quadratic in the fermionic operators like the fermion density, we are entitled to neglect them to leading order in density and treat d_L as a bosonic annihilation operator.

In this approximation, the time evolution is governed by the effective bosonic Hamiltonian of the form

$$H_B = \sum_L E_L d_L^\dagger d_L + \Omega_L (d_L + d_L^\dagger). \quad (7)$$

Starting from the initial FV $|0^+\rangle$, the time-evolved state can be written as a many-mode coherent state [39]

$|\text{coh}; \alpha_L\rangle = \exp\{\sum_L [\alpha_L d_L^\dagger - \alpha_L^* d_L]\} |0^+\rangle$ with amplitudes [35]

$$\alpha_L = \frac{\Omega_L}{E_L} (e^{-iE_L t} - 1). \quad (8)$$

Within this Coherent Bubble Theory (CBT), the density of the bosonic bubbles is

$$\mathcal{N}(t) = \sum_L \frac{\langle d_L^\dagger d_L \rangle(t)}{N} = \sum_L \frac{4\Omega_L^2}{N} \frac{\sin^2(E_L t/2)}{E_L^2}. \quad (9)$$

Since the coupling Ω_L is proportional to \sqrt{N} [35] and decreases exponentially for large L , the bubble density \mathcal{N} is indeed independent of the system size N . The bubble density has a further interest as it is related to the FV survival probability $\mathcal{P}(t)$ through

$$\mathcal{P}(t) = |\langle 0^+ | \psi(t) \rangle|^2 = e^{-N\mathcal{N}(t)}. \quad (10)$$

In appropriate regimes, $\mathcal{N}(t)$ is experimentally accessible by measuring the number of TV bubbles after a given time. The CBT also allows to estimate [35] the density $P_n(t)$ of bubbles of a given size n , from which the TV density is approximately given by

$$\rho(t) = \sum_{n=1}^N n P_n(t), \quad (11)$$

and the connected spin-spin correlation function can be estimated as

$$\begin{aligned} C_n(t) &= \frac{1}{N} \sum_{m=1}^N (\langle \sigma_{n+m}^x \sigma_m^x \rangle - \langle \sigma_m^x \rangle^2) \\ &\approx 4M^2 \sum_{l=n+1}^N (l-n) P_l(t). \end{aligned} \quad (12)$$

As a first step, we have benchmarked the predictions of the CBT against MPS simulations, finding good agreement for all parameter sets presented. Examples of such comparisons are shown in the End Matter.

Results for the rigid regime – The results for the RB regime are shown in Fig. 2.a–d. The time-evolution of the bubble density in Fig. 2.a displays signatures of the discreteness of the energy levels and the exponential decay of the coupling Ω_L for growing L shown in Fig. 1.b: the strongly coupled high-energy modes give rise to rapid oscillations (see inset in Fig. 2.a) superimposed on the slow dynamics governed by the low-energy near-resonant eigenstate. As a consequence of the well defined size l_r of the resonant bubble, the TV density ρ in Fig. 2.b differs from the bubble density \mathcal{N} only by a constant prefactor; the correlation functions in Fig. 2.c,d have a rigid envelope that does not extend beyond l_r . On the other hand, the temporal evolution of the bubble density (and, thus, of the magnitude of the correlation signal) displays a strong dependence on the parameters via

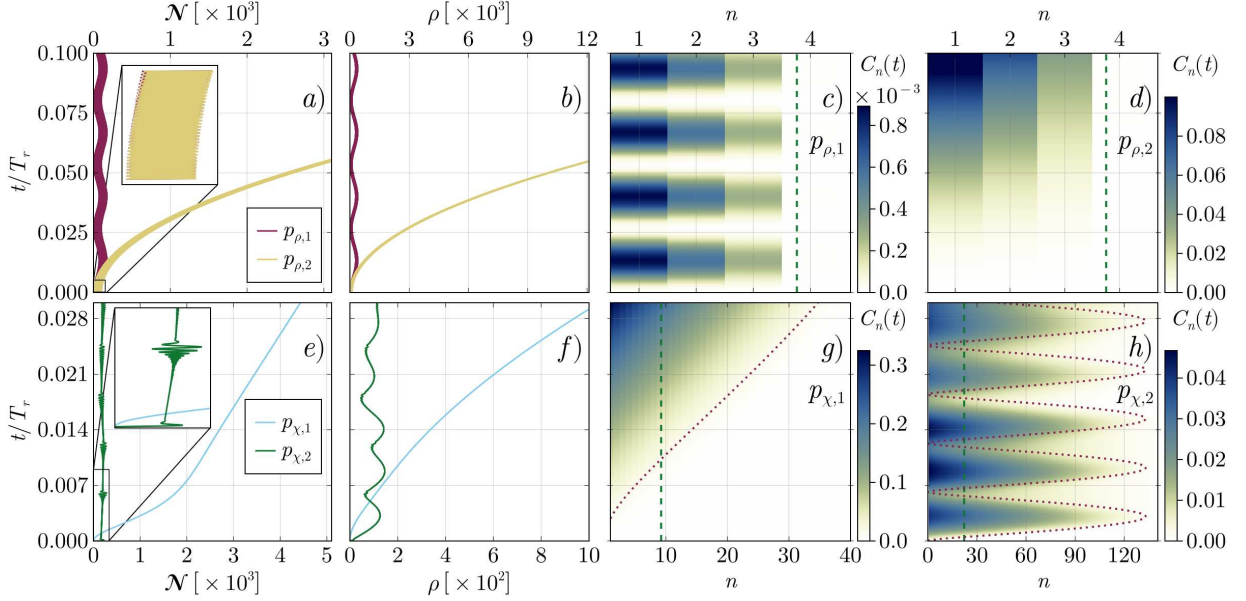


FIG. 2. Time evolution from the coherent bubble theory (CBT) for the parameter sets discussed in Fig. 1. *a + e*) shows the bubble density $\mathcal{N}(t)$ in Eq. (9). The insets show the short time behavior. *b + f*) are plots of the approximated TV density $\rho(t)$ in Eq. (11). $\{c, d, g, h\}$ are the approximated spin-spin correlation functions in Eq. (12). The dashed vertical lines represent the classical resonant bubble size l_r while the dotted lines show the semi-classical bubble expansion dynamics $r(t)$ of Eq. (13).

the exact value of E_r . For the parameters $p_{\rho,1}$, the near-resonant mode has a small, yet finite energy $E_r \neq 0$ that sets the frequency of the persistent oscillations between the vacuum state $|0^+\rangle$ and the near-resonant eigenstate that are visible in Fig. 2.(a-c). With the careful tuning of the parameters of $p_{\rho,2}$, we can set $E_r = 0$. In this exactly resonant case, the slow dynamics of the bubble density exhibits a quadratic growth in time, $\mathcal{N}_r(t) = \Omega_r^2 t^2 / N$; this is reflected in the corresponding increase of the magnitude of the correlations and in a super-exponential decay of the FV survival probability Eq. (10). Even though their size is locked to l_r , their increasing density causes the bubbles to start interacting at long times. At this point, the fermionic correction in Eq. (6) are important, resulting in a breakdown of the CBT and the likely onset of thermalization behaviors.

Results for the expandable regime – In the XB regime, the single-bubble eigenstates become significantly denser in both energy and coupling strength as one can see in Fig. 1.a-b. As a result, many such eigenstates now possess comparable energies and couplings, leading to the qualitatively different dynamical behavior shown in Fig. 2.e-h. Focusing first on the parameter set $p_{\chi,1}$, the bubble density in Fig. 2.e displays a quick transient due to the high-energy eigenstates followed by a slower evolution characterized by a linear increase in time. This behavior emerges because the characteristic energy scale over which $|\Omega_L|^2$ appears approximately flat –corresponding via Eq. (4) to the timescale $T_\Omega = (1 - h_\perp)/(J|h_\parallel|M)$ – is much shorter than the timescale

set by the discreteness of the energy levels, $T_\Delta = \Delta E^{-1}$. This creates a time window $T_\Omega < t_{\text{FVD}} < T_\Delta$, during which the initial state effectively couples to a continuum of modes, resulting in a Fermi’s Golden Rule (FGR)-type dynamics. Most importantly, note how this FGR dynamics does not require any interaction-induced broadening of the eigenstates as it was instead done in [33], but naturally stems from the dense nature of the eigenstates.

An immediate consequence of this linear growth is the exponential decrease of the FV survival probability Eq. (10), which is a defining feature of FVD physics. On top of this, the super-linear growth of the TV density ρ in Fig. 2.f signals that the bubbles do expand after being created. This is in agreement with Coleman’s original picture [28] and is also clearly visible in the analogous expansion of the spin correlation function. The bubble expansion speed is determined by the maximum speed at which the fermionic excitations can move, as indicated by the dashed line in Fig. 2.g.

The basic FVD dynamics eventually breaks down at long times due to two possible mechanisms. The first is the onset of interactions between bubbles: as the density and the size of the bubbles grow, the assumptions underlying the CBT are no longer valid. Comparison with numerical MPS calculations for this parameter choice shows that for $\rho = 0.1$ the relative error in the magnetization is around 3.4% (see End Matter) but rapidly increases for longer time. While on very long times interactions between bubbles are crucial for the system to thermalize [34], the recent work [8] has related the FVD dy-

namics to the exponential decay of the magnetization, which requires an interaction-induced broadening of the two-fermion eigenstates on an intermediate time-scale. In contrast, we find that FVD occurs at much earlier times when interactions are still negligible, giving bubble nucleation at a constant spatio-temporal rate and an exponential decrease of the FV survival probability, in full agreement with the original Coleman’s picture [28].

The second mechanism is peculiar to the discrete geometry of the chain, as first pointed out in [40]. Given the periodicity of the fermionic dispersion relation in a lattice, within a semiclassical picture the expansion dynamics of a single isolated bubble displays Bloch oscillations of the bubble size,

$$r(t) = \frac{1}{M|h_{\parallel}|} [\epsilon(2JM|h_{\parallel}|t) - \epsilon(0)], \quad (13)$$

whose turning points approximately correspond to the extremes of the l_r^{\pm} of the resonant eigenfunction.

This physics is hardly visible in the parameter set $p_{\chi,1}$ as the FV density grows outside the validity range of our CBT well before the onset of Bloch oscillations. To probe it, we need to slow down the FVD dynamics compared to the Bloch oscillation one. This is done in the parameter set $p_{\chi,2}$: by reducing h_{\parallel} , the FVD rate is exponentially suppressed while the Bloch oscillation period increases by a moderate factor around two.

In Fig. 2.e, the strong initial increase of the bubble density \mathcal{N} is again due to the high energy modes and is followed by an approximately linear FVD-like behavior (see inset). At longer times, however, the discreteness of the single-bubble eigenstates emerges again, making the FGR approximation inaccurate. This leads to the Bloch-oscillation-like behavior of the TV density shown in Fig. 2.f.

Even clearer signatures are observed in the correlation function shown in Fig. 2.h. Here, the bubble size predicted by the Bloch oscillations Eq. (13) is indicated by the dashed line and qualitatively agrees with the edge of the correlation function. After a Bloch period $t_{\text{Bloch}} = 2\pi/(2JM|h_{\parallel}|)$, the first-generated bubbles have contracted again to almost zero size. Of course, as the time progresses the Bloch oscillation of bubbles generated at different times give rise to an overall growth of the background correlation signal which extends up to the maximum bubble size l_r^+ . As the Bloch oscillations stem from the discrete lattice geometry, it can be suppressed by reducing the lattice spacing so as to increase the period and the extension of the Bloch oscillations, and thus approach a continuous Ising field theory [25].

Conclusions – In this work we have reported a general theoretical study of the relaxation dynamics of a ferromagnetic spin-1/2 chain in response to a quench of an external longitudinal magnetic field. Using a novel bosonic description of the coherent bubble dynamics, we have

identified very different behaviors depending on the bubble rigidity. In particular, a regime displaying an exponential decay of the survival probability of the false vacuum and a quick bubble expansion process is observed. These results are in full agreement with Coleman’s original picture [28] of a stochastic nucleation of isolated bubbles at a given spatio-temporal rate followed by a bubble expansion at relativistic speed. Going beyond the literature [8], the success of our theory shows that the false vacuum decay process in quantum spin chains is independent from bubble interactions. Furthermore, our approach naturally bridges the false vacuum decay process to the Bloch oscillation physics arising from the lattice [40].

While our coherent bubble theory is restricted to moderate times when bubbles are too dilute to interact, relaxing this approximation will provide a tool to explain the late-time exponential relaxation of the magnetization going beyond the rigid bubble description used so far. Other interesting directions will be to extend our theory to more complex spin models [41], in particular spin-1 chains that also include bosonic spin-wave excitation modes. This will enrich the model by allowing for spontaneous particle emission processes at the fast-moving bubble interface in connection to white- and black-hole horizon physics [25].

An independent study [42] with complementary results appeared on the same day as this submission.

Acknowledgement We acknowledge useful discussions with Karel Van Acoleyen, Federica Surace and Vyacheslav Rychkov. This work has been supported by the Provincia Autonoma di Trento; by the Q@TN Initiative; by the National Quantum Science and Technology Institute through the PNRR MUR Project under Grant PE0000023-NQSTI, co-funded by the European Union - NextGeneration EU; by the European Union - NextGeneration EU, within PRIN 2022, PNRR M4C2, Project TANQU 2022FLSPAJ [CUP B53D23005130006]. Part of the numerical calculations for this work have been performed on the “Deeplearning cluster” supported by the initiative “Dipartimenti di Eccellenza 2018-2022 (Legge 232/2016)” funded by the MUR.

End Matter

Comparison to MPS

The time evolution of the infinite spin- $\frac{1}{2}$ chain can be computed numerically using Matrix Product States. We use the iTEBD algorithm [43] and use bond-dimensions large enough for the presented quantities to be converged. To compare the Coherent Boson Theory with the MPS results we approximate the magnetization of the spin

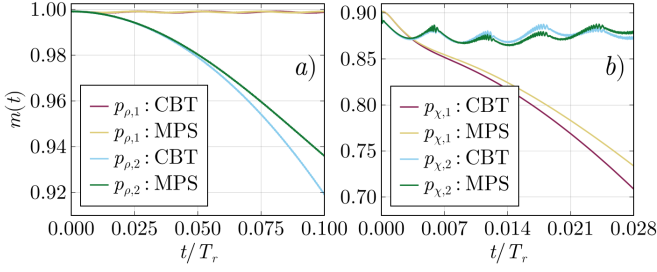


FIG. 3. Comparison between the magnetization approximated in Eq. (14) and the numerically exact MPS calculation with a bond dimension truncation of 1000.

chain within the CBT (see derivation in Supplementary)

$$m(t) = M + \langle G_{\Omega} \rangle(t) + \langle G_{\lambda} \rangle(t). \quad (14)$$

The first contribution arises from the coupling between the false vacuum and one-bubble states

$$\langle G_{\Omega} \rangle(t) = \frac{2}{NJ|h_{\parallel}|} \sum_L \frac{\Omega_L^2}{E_L} [\cos(E_L t) - 1], \quad (15)$$

while the second term is related to the magnetization of a one-bubble eigenstate

$$\langle G_{\lambda} \rangle(t) = \frac{1}{NJ|h_{\parallel}|} \sum_{L,L'} \lambda_{L,L'} \frac{\Omega_L \Omega_{L'}}{E_L E_{L'}} \left(\cos[(E_L - E_{L'})t] - 2 \cos(E_L t) + 1 \right) \quad (16)$$

with

$$\lambda_{L,L'} = -J|h_{\parallel}| 2M \sum_{n=1}^N n \phi_{L,n} \phi_{L',n}. \quad (17)$$

The comparison of the approximated magnetization within the CBT with the numerically converged MPS is shown in Fig. 3. For both $p_{\rho,1}$ and $p_{\chi,2}$ the TV density (see Fig. 2.b,f), remains small in the considered time window. Consequently, the relative error between the MPS and CBT is small and bounded. In this case the error is not dominated by the emergence of interaction but also influenced by the approximated nature of the magnetization operator used in the CBT, which is considered in the $h_{\perp} \rightarrow 0$ limit (see Supplementary). For $p_{\rho,2}$ and $p_{\chi,2}$ the envelope of the TV density grows monotonically. For long times interactions thus becomes important and leads to a breakdown of the CBT. From the magnetization comparison we observe that the CBT overestimates the change in magnetization, indicating that the interactions between bubbles are also repulsive and slows down both the expansion and creation of bubbles. Within the considered time window the maximum relative error of the magnetization $\delta_{\text{mag}} = |m_{\text{CBT}}(t_{\text{max}}) - m_{\text{TN}}(t_{\text{max}})| / |m_{\text{TN}}(t_{\text{max}})|$, is the largest for $p_{\chi,1}$ but still remains below 3.5%, keeping

the CBT prediction close to the converged MPS results for all the presented data in the main text.

The good agreement seen for the magnetization also holds for the correlation function in Eq. (12). In Fig. 4 the CBT correlation functions from Fig. 2 are plotted above the same correlation functions computed with MPS. The agreement is remarkably good considering the simple nature of the approximation used to derive the CBT result [35]. The benchmarking against MPS therefore shows that the CBT predictions provide a good quantitative approximation to the full time evolution of the quenched model.

* christianhoj.johansen@ino.cnr.it

† alessio.recati@cnr.it

‡ iacopo.carusotto@ino.cnr.it

§ alberto.biella@cnr.it

- [1] J. S. Langer, *Statistical Theory of the Decay of Metastable States*, Vol. 54 (Elsevier, 1969) pp. 258–275.
- [2] K. Macieszczak, M. Guta, I. Lesanovsky, and J. P. Garrahan, *Physical Review Letters* **116**, 240404 (2016).
- [3] C. Yin, F. M. Surace, and A. Lucas, *Physical Review X* **15**, 011064 (2025), also available as arXiv:2408.05261v2 [math-ph].
- [4] R. W. Gurney and E. U. Condon, *Nature* **122**, 439 (1928).
- [5] K. Krane, *Introductory Nuclear Physics* (Wiley, 1991).
- [6] P. G. Debenedetti, (1996).
- [7] D. W. Oxtoby, *Journal of Physics: Condensed Matter* **4**, 7627 (1992).
- [8] G. Lagnese, F. M. Surace, M. Kormos, and P. Calabrese, *Phys. Rev. B* **104**, L201106 (2021).
- [9] F. Devoto, S. Devoto, L. Di Luzio, and G. Ridolfi, *Journal of Physics G: Nuclear and Particle Physics* **49**, 103001 (2022).
- [10] A. Zenesini, A. Berti, R. Cominotti, C. Rogora, I. G. Moss, T. P. Billam, I. Carusotto, G. Lamporesi, A. Recati, G. Ferrari, and et al., *Nature Physics* **20**, 558 (2024).
- [11] J. Vodeb, J.-Y. Desaulles, A. Hallam, A. Rava, G. Humar, D. Willsch, F. Jin, M. Willsch, K. Michielsen, and Z. Papić, *Nature physics* **21**, 386 (2025).
- [12] Z.-H. Zhu, Y. Liu, G. Lagnese, F. M. Surace, W.-Y. Zhang, M.-G. He, J. C. Halimeh, M. Dalmonte, S. C. Morampudi, F. Wilczek, Z.-S. Yuan, and J.-W. Pan, “Probing false vacuum decay on a cold-atom gauge-theory quantum simulator,” (2024), arXiv:2411.12565 [cond-mat.quant-gas].
- [13] S. Sachdev, *Quantum Phase Transitions*, 2nd ed. (Cambridge University Press, 2011).
- [14] P. Pfeuty, *Annals of Physics* **57**, 79 (1970).
- [15] R. Coldea, D. A. Tennant, E. M. Wheeler, E. Wawrzynska, D. Prabhakaran, M. Telling, K. Habicht, P. Smeibidl, and K. Kiefer, *Science* **327**, 177 (2010), <https://www.science.org/doi/pdf/10.1126/science.1180085>.
- [16] E. Altman, K. R. Brown, G. Carleo, L. D. Carr, E. Demler, C. Chin, B. DeMarco, S. E. Economou, M. A. Eriksson, K.-M. C. Fu, M. Greiner, K. R. Hazzard, R. G. Hulet, A. J. Kollár, B. L. Lev, M. D. Lukin, R. Ma,

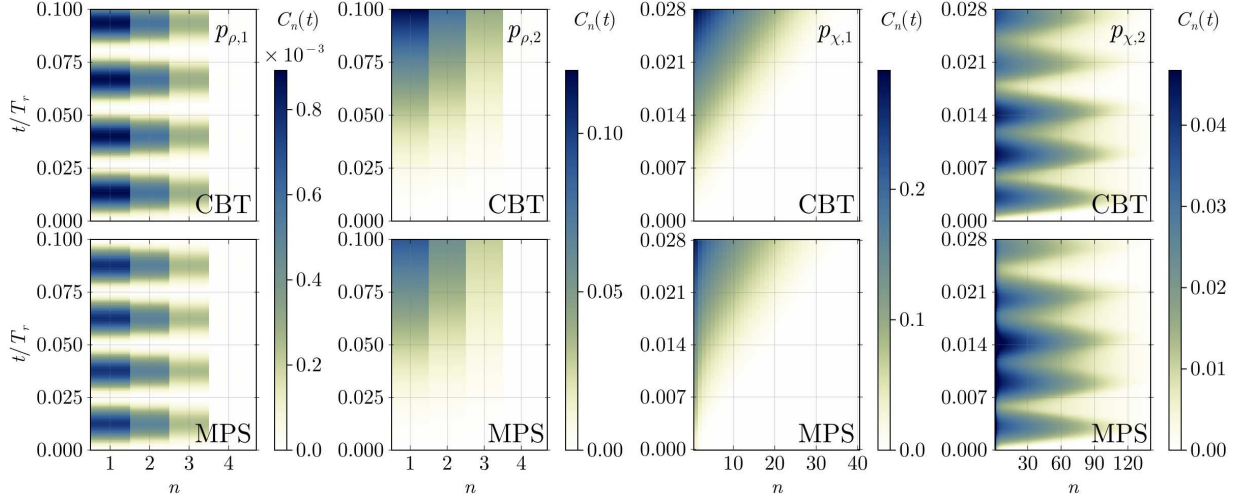


FIG. 4. Comparison between the approximated spin-spin correlation functions within the CBT (upper row) with the numerical ones computed with Matrix Product States (lower row).

- X. Mi, S. Misra, C. Monroe, K. Murch, Z. Nazario, K.-K. Ni, A. C. Potter, P. Roushan, M. Saffman, M. Schleier-Smith, I. Siddiqi, R. Simmonds, M. Singh, I. Spielman, K. Temme, D. S. Weiss, J. Vučković, V. Vuletić, J. Ye, and M. Zwerlein, [PRX Quantum](#) **2**, 017003 (2021).
- [17] C. W. Bauer, Z. Davoudi, A. B. Balantekin, T. Bhattacharya, M. Carena, W. A. de Jong, P. Draper, A. El-Khadra, N. Gemelke, M. Hanada, D. Kharzeev, H. Lamm, Y.-Y. Li, J. Liu, M. Lukin, Y. Meurice, C. Monroe, B. Nachman, G. Pagano, J. Preskill, E. Rinaldi, A. Roggero, D. I. Santiago, M. J. Savage, I. Siddiqi, G. Siopsis, D. Van Zanten, N. Wiebe, Y. Yamauchi, K. Yeter-Aydeniz, and S. Zorzetti, [PRX Quantum](#) **4**, 027001 (2023).
- [18] A. De, A. Lerose, D. Luo, F. M. Surace, A. Schuckert, E. R. Bennewitz, B. Ware, W. Morong, K. S. Collins, Z. Davoudi, A. V. Gorshkov, O. Katz, and C. Monroe, “Observation of string-breaking dynamics in a quantum simulator,” (2024), [arXiv:2410.13815 \[quant-ph\]](#).
- [19] A. Keesling, A. Omran, H. Levine, H. Bernien, H. Pichler, S. Choi, R. Samajdar, S. Schwartz, P. Silvi, S. Sachdev, *et al.*, *Nature* **568**, 207 (2019).
- [20] F. M. Surace and O. Motrunich, [PRX Quantum](#) **5**, 010317 (2024).
- [21] K. L. Ng, B. Opanchuk, M. Thenabadu, M. Reid, and P. D. Drummond, [PRX Quantum](#) **2**, 010350 (2021).
- [22] T. P. Billam, K. Brown, and I. G. Moss, [Phys. Rev. A](#) **102**, 043324 (2020).
- [23] P. Silvi, F. Tschirsich, M. Gerster, J. Jünemann, D. Jaschke, M. Rizzi, and S. Montangero, *SciPost Physics Lecture Notes*, 008 (2019).
- [24] J. Maki, A. Berti, I. Carusotto, and A. Biella, [SciPost Phys.](#) **15**, 152 (2023), [arXiv:arXiv:2306.01067 \[quant-ph\]](#).
- [25] G. Lagnese, F. M. Surace, S. Morampudi, and F. Wilczek, “Detecting a long lived false vacuum with quantum quenches,” (2023), [arXiv:2308.08340 \[cond-mat.stat-mech\]](#).
- [26] A. Lerose, F. M. Surace, P. P. Mazza, G. Peretto, M. Collura, and A. Gambassi, [Phys. Rev. B](#) **102**, 041118 (2020).
- [27] F. M. Surace and A. Lerose, [New Journal of Physics](#) **23**, 062001 (2021).
- [28] S. Coleman, [Phys. Rev. D](#) **15**, 2929 (1977).
- [29] E. Lieb, T. Schultz, and D. Mattis, [Annals of Physics](#) **16**, 407 (1961).
- [30] S. Pikin and V. Tsukernik, [Soviet Physics JETP](#) **23** (1966).
- [31] B. M. McCoy, [Phys. Rev.](#) **173**, 531 (1968).
- [32] R. Verdel, F. Liu, S. Whitsitt, A. V. Gorshkov, and M. Heyl, [Phys. Rev. B](#) **102**, 014308 (2020).
- [33] S. B. Rutkevich, [Phys. Rev. B](#) **60**, 14525 (1999).
- [34] S. Birnkammer, A. Bastianello, and M. Knap, [Nature Communications](#) **13**, 7663 (2022).
- [35] See Supplemental Material at URL-will-be-inserted-by-publisher.
- [36] C. Kittel, *Quantum Theory of Solids* (Wiley, 1963).
- [37] H. Haken, *Quantum Field Theory of Solids: An Introduction* (North-Holland, 1976).
- [38] M. C. Tichy, P. A. Bouvrie, and K. Mølmer, [Applied Physics B](#) **117**, 785 (2014).
- [39] R. J. Glauber, [Phys. Rev.](#) **131**, 2766 (1963).
- [40] O. Pomponio, M. A. Werner, G. Zarand, and G. Takacs, [SciPost Phys.](#) **12**, 061 (2022).
- [41] O. Pomponio, A. Krasznai, and G. Takács, *SciPost Physics* **18**, 082 (2025).
- [42] D. Maertens, J. Haegeman, and K. Van Acoleyen, “Real-time bubble nucleation and growth for false vacuum decay on the lattice,” (2025), [arXiv:2508.xxxx](#).
- [43] G. Vidal, [Phys. Rev. Lett.](#) **98**, 070201 (2007).

Supplementary material

Many-body theory of false vacuum decay in quantum spin chains

Christian Johansen,^{1,*} Alessio Recati,^{1,2,†} Iacopo Carusotto,^{1,2,‡} and Alberto Biella^{1,2,§}

¹*Pitaevskii BEC Center, CNR-INO and Dipartimento di Fisica, Università di Trento, Trento, Italy*

²*INFN-TIFPA, Trento Institute for Fundamental Physics and Applications, I-38123 Trento, Italy*

(Dated: August 20, 2025)

In this supplementary material we will derive the Coherent Boson Theory (CBT) starting from the transverse-field Ising model. In Section I we briefly discuss the mapping of the spin Hamiltonian to a fermion model. Following this, Section II summarizes the two fermion states. These first two section closely follow the work in [S1], but are included here to give a self-consistent representation. Using the results from the previous section we then develop the CBT in Section III.

I. THERMODYNAMIC LIMIT AND FERMION MAPPING

We consider one-dimensional chain with N sites. The Hamiltonian under consideration is the transverse-field Ising model quenched by a weak longitudinal field

$$H(t) = -J \left(\sum_{n=1}^{N-1} \sigma_n^x \sigma_{n+1}^x + h_{\perp} \sum_{n=1}^N \sigma_n^z + \theta(t) h_{\parallel} \sum_{n=1}^N \sigma_n^x \right), \quad (\text{S1})$$

where $\theta(t)$ is the Heaviside function. Prior to the quench, the system is diagonalized by a Jordan-Wigner transformation followed by a Fourier and a Bogoliubov transformation [S2]. The diagonalized prequench Hamiltonian takes the form

$$H(t < 0) = \sum_k \epsilon_k \tilde{\gamma}_k^{\dagger} \tilde{\gamma}_k, \quad (\text{S2})$$

where $k \in \{\pm \frac{(2n-1)\pi}{N}, n = 1, \dots, N/2\}$ and $\tilde{\gamma}_k$ is a fermionic annihilation operator, while ϵ_k is the dispersion relation given by

$$\epsilon_k = 2J \sqrt{1 - 2h_{\perp} \cos(k) + h_{\perp}^2}. \quad (\text{S3})$$

The annihilation operators obey the fermionic anti-commutation relations

$$\{\tilde{\gamma}_q, \tilde{\gamma}_k\} = \{\tilde{\gamma}_q^{\dagger}, \tilde{\gamma}_k^{\dagger}\} = 0, \quad \{\tilde{\gamma}_k, \tilde{\gamma}_q^{\dagger}\} = \delta_{q,k}. \quad (\text{S4})$$

The ground state of the prequenched system is two-fold degenerate (for $h_{\perp} < J$) and leads to a spontaneous symmetry breaking with the spins having a projection onto the longitudinal axis of either $\pm M = \pm (1 - h_{\perp}^2)^{1/8}$. The excitations represented by the $\tilde{\gamma}_k^{\dagger}$ correspond to the creation of a delocalized kink [S2]. The width of the delocalized kink, in units of the lattice distance, can be approximated as [S3]

$$W \approx \frac{\sqrt{h_{\perp}}}{1 - h_{\perp}} \quad (\text{S5})$$

Considering the thermodynamic limit, the momentum spacing (Δ_k) becomes infinitesimal and thus leads to the

* christianhoj.johansen@ino.cnr.it

† alessio.recati@cnr.it

‡ iacopo.carusotto@ino.cnr.it

§ alberto.biella@cnr.it

following relations

$$\begin{aligned}
\delta_{n \% N} &= \lim_{N \rightarrow \infty} \frac{1}{N} \sum_k e^{ikn} = \int_{-\pi}^{\pi} \frac{d\theta}{2\pi} e^{i\theta n}, \\
\lim_{N \rightarrow \infty} \frac{\delta_k}{\Delta_k} &= \delta(\theta) = \lim_{N \rightarrow \infty} \frac{1}{\Delta_k N} \sum_n e^{i\theta n}, \\
\lim_{N \rightarrow \infty} \frac{1}{\Delta_k} &= \delta(0), \\
\Delta_k &= \frac{2\pi}{N}.
\end{aligned} \tag{S6}$$

For a more streamlined notation the periodic nature of the discrete Kronecker delta will not be written explicitly. In the thermodynamic limit the $\tilde{\gamma}'$'s obey the anti-commutation relations

$$\{\tilde{\gamma}(\theta), \tilde{\gamma}^\dagger(\theta')\} = \Delta_k \delta(\theta - \theta'), \tag{S7}$$

while the Hamiltonian in Eq. (S2) takes the form

$$\lim_{N \rightarrow \infty} H(t < 0) = \int_{-\pi}^{\pi} \frac{d\theta}{\Delta_k} \epsilon(\theta) \tilde{\gamma}^\dagger(\theta) \tilde{\gamma}(\theta), \tag{S8}$$

where $\epsilon(\theta)$ is functionally identical to Eq. (S3). To find an explicitly N -independent form of $H(t < 0)$, one can introduce rescaled operators: $\gamma(\theta) = \sqrt{N} \tilde{\gamma}(\theta)$. In these operators the Hamiltonian takes the form

$$\lim_{N \rightarrow \infty} H(t < 0) = \int_{-\pi}^{\pi} \frac{d\theta}{2\pi} \epsilon(\theta) \gamma^\dagger(\theta) \gamma(\theta), \tag{S9}$$

and the operators obey the anti-commutation relations

$$\{\gamma(\theta), \gamma(\phi)\} = N \{\tilde{\gamma}(\theta), \tilde{\gamma}(\phi)\} = 2\pi \delta(\theta - \phi). \tag{S10}$$

The corresponding real-space operators are

$$b_n = \frac{1}{N} \int_{-\pi}^{\pi} \frac{d\theta}{\Delta_k} e^{-i\theta n} \gamma(\theta) = \int_{-\pi}^{\pi} \frac{d\theta}{2\pi} e^{-i\theta n} \gamma(\theta), \tag{S11}$$

and obey the anti-commutation relations

$$\{\tilde{b}_n, \tilde{b}_m^\dagger\} = \delta_{n,m}. \tag{S12}$$

Due to the finite lattice spacing the the inverse Fourier transformation remains discrete

$$\gamma(\theta) = \sum_{n=1}^N e^{in\theta} b_n. \tag{S13}$$

In the thermodynamic limit the quenched Hamiltonian can also be written in the fermion basis [S1]

$$H(t > 0) = H(t < 0) + V \tag{S14}$$

with

$$V = J |h_{\parallel}| M \sum_{n=1}^N : \exp \left(- \sum_{j < n}^N \psi_j^{(+)} \psi_j^{(-)} \right) :, \tag{S15}$$

where $:$ symbolizes normal-ordering and

$$\psi_j^{(+)} = i \int_{-\pi}^{\pi} \frac{d\theta}{\sqrt{2\pi}} \frac{e^{ij\theta}}{\sqrt{\epsilon(\theta)}} [\gamma(\theta) + \gamma^\dagger(-\theta)], \quad \psi_j^{(-)} = i \int_{-\pi}^{\pi} \frac{d\theta}{\sqrt{2\pi}} e^{ij\theta} \sqrt{\epsilon(\theta)} [-\gamma(\theta) + \gamma^\dagger(-\theta)]. \tag{S16}$$

One can split V into two contributions: one that conserves the kink number V_0 and the rest which couples sectors with different number of kinks. The simplest way of achieving this is to define V_0 in the flat-dispersion limit [S1]

$$V_0 = \lim_{h_\perp \rightarrow 0} V = J|h_\parallel| M \sum_{n=1}^N : \exp \left(-2 \sum_{j < n} b_j^\dagger b_j \right) : . \quad (\text{S17})$$

One can thus reorder the quenched Hamiltonian into the form

$$H(t > 0) = H_0 + \tilde{V}, \quad (\text{S18})$$

where $H_0 = H(t < 0) + V_0$ and $\tilde{V} = V - V_0$. As V_0 does not couple different kink sectors, coupling between sectors with different fermion number is fully described by V . One notices that since this is normal-ordered exponential of an even number of γ 's, V can only add or remove an even number of fermions. Considering quenches from $|0_+\rangle$ means that for $t < 0$ there are no fermions in the system and for $t > 0$ one will thus only find states with an even number of fermions.

II. TWO-FERMION STATES

If one considers either small longitudinal field or small transverse field, then \tilde{V} only weakly couples sectors with different fermion numbers. This creates a time scale where the system can be approximated by a truncated Hilbert space consisting of the ground state and a single two-fermion state. The two-fermion states has to conserve momentum and we can thus describe the l 'th two-fermion state as

$$|\phi_L\rangle = \mathcal{N} \int_{-\pi}^{\pi} d\theta \phi_L(\theta) \gamma^\dagger(\theta) \gamma^\dagger(-\theta) |0_+\rangle. \quad (\text{S19})$$

These states are eigenstates of the two-body problem with eigenenergies E_L

$$H_0 |\phi_L\rangle = E_L |\phi_L\rangle. \quad (\text{S20})$$

The normalization \mathcal{N} is defined through the overlap

$$\langle \phi_L | \phi_{L'} \rangle = \mathcal{N}^2 \int_{-\pi}^{\pi} d\theta d\phi \phi_L^*(\theta) \phi_{L'}(\phi) \langle 0_+ | \mathcal{M}_\gamma(\theta, \phi) | 0_+ \rangle = 1. \quad (\text{S21})$$

The operator product

$$\mathcal{M}_\gamma(\theta, \phi) = \gamma(-\theta) \gamma(\theta) \gamma^\dagger(\phi) \gamma^\dagger(-\phi) \quad (\text{S22})$$

inside the FV expectation value will be important again later so we therefore normal-order it here.

$$\begin{aligned} \mathcal{M}_\gamma &= \gamma(-\theta) [N\Delta_k \delta(\theta - \phi) - \gamma^\dagger(\phi) \gamma(\theta)] \gamma^\dagger(-\phi), \\ &= (N\Delta_k^2) \delta(\theta - \phi)^2 - N\Delta_k \delta(\theta - \phi) \gamma^\dagger(-\phi) \gamma(-\theta) - N\Delta_k \delta(\theta + \phi) \gamma(-\theta) \gamma^\dagger(\phi) + \gamma(-\theta) \gamma^\dagger(\phi) \gamma^\dagger(-\phi) \gamma(\theta), \\ &= (N\Delta_k)^2 \delta(\theta - \phi)^2 - N\Delta_k \delta(\theta - \phi) \gamma^\dagger(-\phi) \gamma(-\theta) - (N\Delta_k)^2 \delta(\theta + \phi)^2 + N\Delta_k \delta(\theta + \phi) \gamma^\dagger(\phi) \gamma(-\theta) \\ &\quad + N\Delta_k \delta(\theta + \phi) \gamma^\dagger(-\phi) \gamma(\theta) - \gamma^\dagger(\phi) \gamma(-\theta) \gamma^\dagger(-\phi) \gamma(\theta), \\ &= (N\Delta_k)^2 \delta(\theta - \phi)^2 - N\Delta_k \delta(\theta - \phi) \gamma^\dagger(-\phi) \gamma(-\theta) - (N\Delta_k)^2 \delta(\theta + \phi)^2 + \Delta_k \delta(\theta + \phi) \gamma^\dagger(\phi) \gamma(-\theta) \\ &\quad + (N\Delta_k) \delta(\theta + \phi) \gamma^\dagger(-\phi) \gamma(\theta) - N\Delta_k \delta(\theta - \phi) \gamma^\dagger(\phi) \gamma(\theta) + \gamma^\dagger(\phi) \gamma^\dagger(-\phi) \gamma(-\theta) \gamma(\theta). \end{aligned} \quad (\text{S23})$$

When evaluating $\langle 0_+ | \mathcal{M}_\gamma | 0_+ \rangle$ all but two terms vanish as γ annihilates the state when applied to $|0_+\rangle$:

$$\begin{aligned} \langle \phi_L | \phi_{L'} \rangle &= (N\Delta_k)^2 \mathcal{N}^2 \int_{-\pi}^{\pi} d\theta d\phi \phi_L^*(\theta) \phi_{L'}(\phi) [\delta(\theta - \phi)^2 - \delta(\theta + \phi)^2], \\ &= (N\Delta_k)^2 \mathcal{N}^2 \int_{-\pi}^{\pi} d\theta \delta(0) [\phi_L^*(\theta) \phi_{L'}(\theta) - \phi_L^*(\theta) \phi_{L'}(-\theta)]. \end{aligned} \quad (\text{S24})$$

The combination of the symmetric momentum interval and the exclusion principle can be used to relate $\phi_L(\theta)$ to $\phi_L(-\theta)$. First by just using the symmetric interval we can express the state as

$$|\phi_L\rangle = \mathcal{N} \int_{-\pi}^{\pi} d\theta \phi_L(\theta) \gamma^\dagger(\theta) \gamma^\dagger(-\theta) |0_+\rangle = \mathcal{N} \int_{-\pi}^{\pi} d\theta \phi_L(-\theta) \gamma^\dagger(-\theta) \gamma^\dagger(\theta) |0_+\rangle. \quad (\text{S25})$$

However, using the anti-commuting property of the creation operators we can also express it as

$$|\phi_L\rangle = \mathcal{N} \int_{-\pi}^{\pi} d\theta \phi_L(\theta) \gamma^\dagger(\theta) \gamma^\dagger(-\theta) |0_+\rangle = -\mathcal{N} \int_{-\pi}^{\pi} d\theta \phi_L(\theta) \gamma^\dagger(-\theta) \gamma^\dagger(\theta) |0_+\rangle. \quad (\text{S26})$$

As the two expression must be equal we see that $\phi_L(\theta) = -\phi_L(-\theta)$. The normalization thus takes the form

$$\begin{aligned} \langle \phi_L | \phi_{L'} \rangle &= 2(N\Delta_k)^2 \mathcal{N}^2 \int_{-\pi}^{\pi} d\theta \delta(0) \phi_L^*(\theta) \phi_{L'}(\theta), \\ &= 2N^2 \Delta_k \mathcal{N}^2 \int_{-\pi}^{\pi} d\theta \phi_L^*(\theta) \phi_{L'}(\theta). \end{aligned} \quad (\text{S27})$$

When numerically solving the two-body problem we do it for finite N in real-space. In that case the coefficients satisfy the relation

$$\sum_{n=1}^N \phi_{L,n}^* \phi_{L',n} = \delta_{L,L'}. \quad (\text{S28})$$

With this convention the integral in Eq. (S27) can be evaluated

$$\int_{-\pi}^{\pi} d\theta \phi_L^*(\theta) \phi_{L'}(\theta) = \int_{-\pi}^{\pi} d\theta \sum_{n,m} \exp[i\theta(m-n)] \phi_{L,n}^* \phi_{L',m} = 2\pi \sum_n \phi_{L,n}^* \phi_{L',n} = 2\pi \delta_{L,L'}, \quad (\text{S29})$$

giving the normalization $\mathcal{N} = 1/\sqrt{4\pi\Delta_k N^2} = 1/\sqrt{2(2\pi)^2 N}$, such that the momentum space wave-function takes the form

$$|\phi_L\rangle = \frac{1}{\sqrt{2N}} \int_{-\pi}^{\pi} \frac{d\theta}{2\pi} \phi_L(\theta) \gamma^\dagger(\theta) \gamma^\dagger(-\theta) |0_+\rangle. \quad (\text{S30})$$

A. Real-space representation

Having found the momentum space representation of the two-fermion state it can easily be transformed to real space

$$\begin{aligned} |\phi_L\rangle &= \frac{1}{\sqrt{2N}} \sum_{n,m,m'} \int_{-\pi}^{\pi} \frac{d\theta}{2\pi} \exp[i\theta(n+m-m')] \phi_{L,n} b_{m'}^\dagger b_m^\dagger |0_+\rangle, \\ &= \frac{1}{\sqrt{2N}} \sum_{n,m,m'} \delta_{n+m,m'} \phi_{L,n} b_{m'}^\dagger b_m^\dagger |0_+\rangle, \\ &= \frac{1}{\sqrt{2N}} \sum_{n,m} \phi_{L,n} b_{m+n}^\dagger b_m^\dagger |0_+\rangle, \end{aligned} \quad (\text{S31})$$

which is indeed a translation-invariant two-fermion state. The normalization of the state is given as

$$\langle \phi_L | \phi_{L'} \rangle = \frac{1}{2N} \sum_{n,m,n',m'} \phi_{L,n}^* \phi_{L',n'} \langle 0_+ | b_m b_{m+n} b_{m'+n'}^\dagger b_{m'}^\dagger | 0_+ \rangle. \quad (\text{S32})$$

Evaluating the expectation value is again done using the anti-commutation relations

$$\begin{aligned} \langle 0_+ | b_m b_{m+n} b_{m'+n'}^\dagger b_{m'}^\dagger | 0_+ \rangle &= \langle 0_+ | b_m \left(\delta_{m+n,m'+n'} - b_{m'+n'}^\dagger b_{m+n} \right) b_{m'}^\dagger | 0_+ \rangle, \\ &= \delta_{m+n,m'+n'} \delta_{m,m'} - \langle 0_+ | b_m b_{m'+n'}^\dagger b_{m+n} b_{m'}^\dagger | 0_+ \rangle, \\ &= \delta_{m+n,m'+n'} \delta_{m,m'} - \langle 0_+ | b_m b_{m'+n'}^\dagger \delta_{m+n,m'} | 0_+ \rangle, \\ &= \delta_{m+n,m'+n'} \delta_{m,m'} - \delta_{m+n,m'} \delta_{m'+n',m}. \end{aligned} \quad (\text{S33})$$

Inserting this into the normalization

$$\langle \phi_L | \phi_{L'} \rangle = \frac{1}{2N} \sum_{n,m} \left(\phi_{L,n}^* \phi_{L',n} - \sum_{n',m'} \phi_{L,n}^* \phi_{L',n'} \delta_{m',m+n} \delta_{n',-n} \right). \quad (\text{S34})$$

The modulo nature means that $\delta_{n,-n'}$ should be understood as $\delta_{n,N-n}$. As we consider the even fermion sector the boundary conditions are anti-periodic [S2]. Using the ABC one finds

$$\langle \phi_L | \phi_{L'} \rangle = \frac{1}{N} \sum_{n,m} \phi_{L,n}^* \phi_{L',n} = \sum_n \phi_{L,n}^* \phi_{L',n} = \delta_{L,L'}, \quad (\text{S35})$$

which is consistent with normalization we are using.

B. Coupling to FV and magnetization

Due to \tilde{V} the two-fermion states are coupled to the FV. One can compute this coupling analytically [S1, S4]

$$\Omega_L \equiv \langle 0_+ | V | \phi_L \rangle = \frac{1}{2} \sqrt{N} M J |h_{\parallel}| \sum_{n=1}^N h_{\perp}^n \phi_{L,n} = \Omega_L^*. \quad (\text{S36})$$

The potential is also useful to compute the average magnetization of the state through the definition of V

$$\frac{1}{N} \left\langle \sum_{n=1}^N \sigma_n^x \right\rangle = \frac{\langle V \rangle}{N J |h_{\parallel}|}. \quad (\text{S37})$$

Within the truncated Hilbert space of only the FV and a single one-bubble state we can thus write the approximate average magnetization operator as

$$m_{avg} = M |0_+ \rangle \langle 0_+| + \frac{1}{N J |h_{\parallel}|} \sum_{L=1}^N \Omega_L (|0_+ \rangle \langle \phi_L| + |\phi_L \rangle \langle 0_+|) + \frac{1}{N J |h_{\parallel}|} \sum_{L,L'=1}^N \tilde{\lambda}_{L,L'} |\phi_L \rangle \langle \phi_{L'}|, \quad (\text{S38})$$

where we have defined

$$\langle \phi_L | V | \phi_{L'} \rangle \approx \langle \phi_L | V_0 | \phi_{L'} \rangle = \tilde{\lambda}_{L,L'}. \quad (\text{S39})$$

The overlap $\tilde{\lambda}_{L,L'}$ is straight-forward to compute as V_0 is diagonal in the real-space representation [S1] and the overlaps takes the form

$$\begin{aligned} \tilde{\lambda}_{L,L'} &= J |h_{\parallel}| M N \sum_{n=1}^N \phi_{L,n}^* \phi_{L',n} \left(1 - \frac{2n}{N} \right), \\ &= J |h_{\parallel}| M N \sum_{n=1}^N \phi_{L,n} \phi_{L',n} \left(1 - \frac{2n}{N} \right), \\ &= J |h_{\parallel}| M N \delta_{L,L'} - J |h_{\parallel}| M N \sum_{n=1}^N \phi_{L,n} \phi_{L',n} \frac{2n}{N}, \end{aligned} \quad (\text{S40})$$

where we used the fact that the spatial coefficients are real making $\tilde{\lambda}_{L,L'}$ real and symmetric. Using the form found for $\tilde{\lambda}_{L,L'}$ in the magnetization Eq. (S38) one notices that the constant terms can be combined into an identity

$$m_{avg} = \mathbb{1} M + \frac{1}{N J |h_{\parallel}|} \sum_{L=1}^N \Omega_L (|0_+ \rangle \langle \phi_L| + |\phi_L \rangle \langle 0_+|) + \frac{1}{N J |h_{\parallel}|} \sum_{L,L'=1}^N \lambda_{L,L'} |\phi_L \rangle \langle \phi_{L'}|, \quad (\text{S41})$$

with

$$\lambda_{L,L'} = -J |h_{\parallel}| 2M \sum_{n=1}^N n \phi_{L,n} \phi_{L',n}. \quad (\text{S42})$$

III. MANY-BODY THEORY FOR TRANSLATION-INVARIANT BUBBLES

As the system is translation-invariant and infinitely large a single bubble does not affect the magnetization of the system. This is clearly seen by $\lim_{N \rightarrow \infty} \lambda_{L,L'}/N = 0$ and $\lim_{N \rightarrow \infty} \Omega_L/N = 0$. This means that a theory with only a single bubble can only be a good description when the system is described by tiny fluctuations on top of the FV [S5]. Otherwise it is necessary to use a many-body description which allows for a finite bubble-density in the thermodynamic limit.

The simplest conceivable many-theory is based on the infinite size of the system and the fact that the one-bubble states $|\phi_L\rangle$ consists of superpositions of bubbles with finite sizes. For low enough densities one thus expects that the state can be approximated as multiple non-interacting bubbles. Each bubble consists of two fermions, so as long as the bubbles do not interact with each other it should be valid to think of the bubbles as non-interacting bosons. This idea belongs in the broader scope of methods known as cobosonization [S6]. Within this method we define a creation operator for the L 'th bubble state

$$d_L^\dagger = \frac{1}{\sqrt{2N}} \int_{-\pi}^{\pi} \frac{d\theta}{2\pi} \phi_L(\theta) \gamma^\dagger(\theta) \gamma^\dagger(-\theta), \quad (\text{S43})$$

The anti-commutation relations of the fermions in Eq. (S4) directly leads to

$$[d_L^\dagger, d_{L'}^\dagger] = [d_L, d_{L'}] = 0, \quad (\text{S44})$$

while

$$[d_L, d_{L'}^\dagger] = \frac{1}{2N} \int_{-\pi}^{\pi} \frac{d\theta d\theta'}{(2\pi)^2} \phi_L^*(\theta) \phi_{L'}(\theta') [\gamma(-\theta) \gamma(\theta), \gamma^\dagger(\theta') \gamma^\dagger(-\theta')]. \quad (\text{S45})$$

We already did the cumbersome part of the calculation of the commutation relation in Eq. (S23)

$$\begin{aligned} [\gamma(-\theta) \gamma(\theta), \gamma^\dagger(\theta') \gamma^\dagger(-\theta')] &= M_\gamma(\theta, \theta') - \gamma^\dagger(\theta') \gamma^\dagger(-\theta') \gamma(-\theta) \gamma(\theta), \\ &= (N\Delta_k)^2 \delta(\theta - \phi)^2 - N\Delta_k \delta(\theta - \phi) \gamma^\dagger(-\phi) \gamma(-\theta) - (N\Delta_k)^2 \delta(\theta + \phi)^2 + N\Delta_k \delta(\theta + \phi) \gamma^\dagger(\phi) \gamma(-\theta) \\ &\quad + N\Delta_k \delta(\theta + \phi) \gamma^\dagger(-\phi) \gamma(\theta) - N\Delta_k \delta(\theta - \phi) \gamma^\dagger(\phi) \gamma(\theta). \end{aligned} \quad (\text{S46})$$

Inserting this into Eq. (S45) one finds

$$\begin{aligned} [d_L, d_{L'}^\dagger] &= \frac{1}{2N} \int_{-\pi}^{\pi} \frac{d\theta}{(2\pi)^2} \left[(N\Delta_k)^2 \delta(0) \phi_L^*(\theta) \phi_{L'}(\theta) - (N\Delta_k)^2 \delta(0) \phi_L^*(\theta) \phi_{L'}(-\theta) - N\Delta_k \phi_L^*(\theta) \phi_{L'}(\theta) \gamma^\dagger(-\theta) \gamma(-\theta) \right. \\ &\quad \left. + N\Delta_k \phi_L^*(\theta) \phi_{L'}(-\theta) \gamma^\dagger(-\theta) \gamma(-\theta) - N\Delta_k \phi_L^*(\theta) \phi_{L'}(\theta) \gamma^\dagger(\theta) \gamma(\theta) + N\Delta_k \phi_L^*(\theta) \phi_{L'}(-\theta) \gamma^\dagger(\theta) \gamma(\theta) \right], \\ &= \frac{\Delta_k}{2} \int_{-\pi}^{\pi} \frac{d\theta}{(2\pi)^2} \left[N\phi_L^*(\theta) \phi_{L'}(\theta) - N\phi_L^*(\theta) \phi_{L'}(-\theta) - \phi_L^*(\theta) \phi_{L'}(\theta) \gamma^\dagger(-\theta) \gamma(-\theta) \right. \\ &\quad \left. + \phi_L^*(\theta) \phi_{L'}(-\theta) \gamma^\dagger(-\theta) \gamma(-\theta) - \phi_L^*(\theta) \phi_{L'}(\theta) \gamma^\dagger(\theta) \gamma(\theta) + \phi_L^*(\theta) \phi_{L'}(-\theta) \gamma^\dagger(\theta) \gamma(\theta) \right], \\ &= \delta_{L,L'} - \frac{2}{N} \int_{-\pi}^{\pi} \frac{d\theta}{2\pi} \phi_L^*(\theta) \phi_{L'}(\theta) \gamma^\dagger(\theta) \gamma(\theta), \end{aligned} \quad (\text{S47})$$

where the anti-symmetry of $\phi_L(\theta)$ have been exploited. This result clearly shows that bosonic commutation relations emerge when only one bubble is present in the system.

In the real-space representation of the bubble-operator the results is

$$[d_L, d_{L'}^\dagger] = \delta_{L,L'} - \frac{2}{N} \sum_{n,m,m'=1}^N \phi_{L,n}^* \phi_{L',m} b_{m-n+m'}^\dagger b_{m'}. \quad (\text{S48})$$

Considering translation-invariance (and thereby doing the sum over m') one finds

$$[d_L, d_{L'}^\dagger] = \delta_{L,L'} - 2 \sum_{n,m} \phi_{L,n}^* \phi_{L',m} b_{m-n}^\dagger b_0. \quad (\text{S49})$$

One notices that in the $h_\perp \rightarrow 0$ case the fermion wave functions becomes strongly localized $\phi_L, n \approx \delta_{L,n}$. In this case the perturbation to the bosonic commutator becomes

$$\lim_{h_\perp \rightarrow 0} [d_L, d_{L'}^\dagger] = \delta_{L,L'} - 2b_{L-L'}^\dagger b_0, \quad (\text{S50})$$

which is always unity for $L = L'$ but is related to the fermion two-point correlation function for $L \neq L'$.

A. Coherent boson theory

We will now assume that the density of bubbles is small enough that the violation of the bosonic commutation relations in Eq. (S47) can be neglected. Under this assumption the state with n bubbles of type L and m bubbles of type L' is given as

$$|n_L, m_{L'}\rangle = \frac{1}{\sqrt{n!m!}} \left(d_L^\dagger\right)^n \left(d_{L'}^\dagger\right)^m |0_+\rangle. \quad (\text{S51})$$

The Hamiltonian contains the single bubble energies and their coupling to the FV

$$H = \sum_{L=1}^N E_L d_L^\dagger d_L + \Omega_L \left(d_L + d_L^\dagger\right). \quad (\text{S52})$$

The non-interacting nature of the bosons means that we can diagonalize the Hamiltonian using a multi-mode displacement operator

$$D = \bigotimes_L D_L(\alpha_L), \quad (\text{S53})$$

with the single-mode displacement operator being defined as

$$D_L(\alpha) = \exp\left(\alpha d_L^\dagger - \alpha^* d_L\right). \quad (\text{S54})$$

This operator is unitary with

$$D_L^\dagger(\alpha) = D_L^{-1}(\alpha) = D_L(-\alpha), \quad (\text{S55})$$

and its action on the annihilation and creation operators are simple shifts

$$\begin{aligned} D_L^\dagger(\alpha) d_L D_L(\alpha) &= d_L + \alpha, \\ D_L^\dagger(\alpha) d_L^\dagger D_L(\alpha) &= d_L^\dagger + \alpha^*. \end{aligned} \quad (\text{S56})$$

When the displacement operator is applied to the vacuum state it generates a coherent state

$$D_L(\alpha_L) |0_+\rangle = \exp\left(-\frac{1}{2}|\alpha_L|^2\right) \sum_{n=0}^N \frac{\alpha_L^n}{\sqrt{n!}} |n_L\rangle = |\alpha_L\rangle. \quad (\text{S57})$$

As the coherent states constitute an over-complete basis the overlap of two coherent states is finite

$$|\langle\alpha_L|\beta_L\rangle|^2 = \exp\left(-|\alpha_L - \beta_L|^2\right). \quad (\text{S58})$$

Applying the multi-mode displacement operator to the Hamiltonian one finds

$$\begin{aligned} \tilde{H} &= D^\dagger H D, \\ &= \sum_L E_L \left(d_L^\dagger + \alpha_L^*\right) \left(d_L + \alpha_L\right) + \Omega_L \left(d_L^\dagger + d_L + 2\text{Re}(\alpha_L)\right), \\ &= \sum_L E_L d_L^\dagger d_L + E_L |\alpha_L|^2 + 2\text{Re}(\alpha_L) \Omega_L + (\Omega_L + E_L \alpha_L^*) d_L + (\Omega_L + E_L \alpha_L) d_L^\dagger, \end{aligned} \quad (\text{S59})$$

where we will use the tilde to indicate that we are in the displaced basis. The linear terms can be removed by choosing $\alpha_L = -\Omega_L/E_L$, which makes the Hamiltonian diagonal

$$\tilde{H} = \sum_L E_L d_L^\dagger d_L - \frac{\Omega_L^2}{E_L}. \quad (\text{S60})$$

One observes that this Hamiltonian is a simple harmonic oscillator where each mode acquires a shift. As the modes do not interact this shift just leads to an overall phase of the wave-function $\sum_L \Omega_L^2/E_L = \chi$. Any time evolved state can therefore simply be represented as

$$|\tilde{\psi}(t)\rangle = e^{it\chi} \sum_{\{n_L\}} c_{\{n_L\}} \exp\left(-i \sum_L E_L n_L t\right) |n_1, n_2, \dots, n_N\rangle = e^{it\chi} \sum_{\{n_L\}} c_{\{n_L\}} \bigotimes_L \exp(-i E_L n_L t) |n_L\rangle. \quad (\text{S61})$$

For our purpose we are interested in time evolving a specific state, namely, the false vacuum state. Transforming the FV to the diagonal basis is straightforward

$$|\tilde{\psi}(0)\rangle = D^\dagger |0_+\rangle = \bigotimes_L D_L(\Omega_L/E_L) |0_+\rangle = \bigotimes_L |\Omega_L/E_L\rangle = \bigotimes_L \exp\left[-\frac{1}{2} \left(\frac{\Omega_L}{E_L}\right)^2\right] \sum_{n=0}^N \frac{\left(\frac{\Omega_L}{E_L}\right)^n}{\sqrt{n!}} |n_L\rangle, \quad (\text{S62})$$

The coefficients in the wave-function expansion now takes the form

$$\langle \tilde{\psi}(0) | n_1, n_2, \dots, n_N \rangle = \prod_L \exp\left[-\frac{1}{2} \left(\frac{\Omega_L}{E_L}\right)^2\right] \frac{\left(\frac{\Omega_L}{E_L}\right)^{n_L}}{\sqrt{n_L!}}. \quad (\text{S63})$$

As the these coefficients are just a product over the modes the entire time-evolved state is a product state for all times

$$\begin{aligned} |\tilde{\psi}(t)\rangle &= e^{it\chi} \bigotimes_L \exp\left[-\frac{1}{2} \left(\frac{\Omega_L}{E_L}\right)^2\right] \sum_{\{n_L\}} \frac{\left(\frac{\Omega_L}{E_L}\right)^{n_L}}{\sqrt{n_L!}} \exp(-i E_L n_L t) |n_L\rangle, \\ &= e^{it\chi} \bigotimes_L \exp\left[-\frac{1}{2} \left(\frac{\Omega_L}{E_L}\right)^2\right] \sum_{\{n_L\}} \frac{\left(\frac{\Omega_L}{E_L} e^{-i E_L t}\right)^{n_L}}{\sqrt{n_L!}} |n_L\rangle, \\ &= e^{it\chi} \bigotimes_L \left| \frac{\Omega_L e^{-i E_L t}}{E_L} \right\rangle, \end{aligned} \quad (\text{S64})$$

which is just a product state of coherent states. Due to the unitarity of the displacement operator the state is also trivially normalized for all times.

1. Dynamics of excitations

If one considers the number of bubbles in the L 'th state then this is given by

$$\begin{aligned} \langle \psi(t) | d_L^\dagger d_L | \psi(t) \rangle &= \langle \tilde{\psi}(t) | D^\dagger d_L^\dagger D D^\dagger d_L D | \tilde{\psi}(t) \rangle, \\ &= \langle \tilde{\psi}(t) | \left(d_L^\dagger - \frac{\Omega_L}{E_L}\right) \left(d_L - \frac{\Omega_L}{E_L}\right) | \tilde{\psi}(t) \rangle, \\ &= \langle \tilde{\psi}(t) | \left(d_L^\dagger d_L + \left(\frac{\Omega_L}{E_L}\right)^2 - d_L^\dagger \frac{\Omega_L}{E_L} - d_L \frac{\Omega_L}{E_L}\right) | \tilde{\psi}(t) \rangle, \\ &= \left(\frac{\Omega_L}{E_L}\right)^2 (2 - e^{i E_L t} - e^{-i E_L t}), \\ &= 2 \left(\frac{\Omega_L}{E_L}\right)^2 [1 - \cos(E_L t)], \\ &= \left(\frac{2\Omega_L}{E_L}\right)^2 \sin^2(E_L t/2), \end{aligned} \quad (\text{S65})$$

which means that the system initially has no occupation and is therefore consistent with the initial state used. With this result our prediction is that the dynamics of the L 'th bubble has a time-scale directly set by $1/E_L$ but that its "importance"/magnitude in the dynamics is set by $\left(\frac{\Omega_L}{E_L}\right)^2$. As the system is infinite the relevant quantity is not the number of bubbles but instead their density

$$\mathcal{N}_L = \frac{\langle \psi(t) | d_L^\dagger d_L | \psi(t) \rangle}{N} = \frac{1}{N} \left(\frac{2\Omega_L}{E_L} \right)^2 \sin^2(E_L t/2). \quad (\text{S66})$$

Since $\Omega_L \propto \sqrt{N}$ as seen in Eq. (S36) and E_L is an intensive quantity, the density of the L 'th bubble becomes intensive and therefore well-defined in the thermodynamic limit. This observable describes the average number of bubbles of species L at a single site. For the case of a resonant bubble, $E_r \rightarrow 0$ allowing us to expand the sine

$$N_r = \frac{\Omega_r^2 t^2}{N}, \quad (\text{S67})$$

giving the resonant physics a time scale of

$$T_r = \frac{1}{2JM|h_\parallel| \sum_{n=1}^N h_\perp^n \phi_{r,n}}. \quad (\text{S68})$$

2. Average magnetization

To compare the results of the CBT with MPS calculations, we wish to compute an approximation to the average magnetization within the CBT. To compute the magnetization we can directly promote the single-body average magnetization operator in Eq. (S41) to a many body-operator

$$m_{avg} = M + \frac{1}{NJ|h_\parallel|} \sum_{L=1}^N \Omega_L (d_L + d_L^\dagger) + \frac{1}{NJ|h_\parallel|} \sum_{L,L'=1}^N \lambda_{L,L'} d_L^\dagger d_{L'}, \quad (\text{S69})$$

where we remind the reader that there is an additional flat-band approximation in $\lambda_{L,L'}$. Using the same procedure as for the bubble occupation we transform m_{avg} to the displaced basis

$$\begin{aligned} \tilde{m}_{avg} &= D^\dagger m_{avg} D, \\ &= M + \frac{1}{NJ|h_\parallel|} \sum_L \Omega_L \left(d_L + d_L^\dagger - 2\frac{\Omega_L}{E_L} \right) + \frac{1}{NJ|h_\parallel|} \sum_{L,L'} \lambda_{L,L'} \left(d_L^\dagger - \frac{\Omega_L}{E_L} \right) \left(d_{L'} - \frac{\Omega_{L'}}{E_{L'}} \right), \\ &= M + \frac{1}{NJ|h_\parallel|} \sum_L \Omega_L \left(d_L + d_L^\dagger - 2\frac{\Omega_L}{E_L} \right) + \frac{1}{NJ|h_\parallel|} \sum_{L,L'} \lambda_{L,L'} \left[d_L^\dagger d_{L'} - \frac{\Omega_L}{E_L} d_{L'} \right. \\ &\quad \left. - \frac{\Omega_{L'}}{E_{L'}} d_L^\dagger + \frac{\Omega_L \Omega_{L'}}{E_L E_{L'}} \right], \\ &= M + G_\Omega + G_\lambda. \end{aligned} \quad (\text{S70})$$

We can now compute overlaps with the time-dependent state in Eq. (S64) of the two different terms. The first contribution arises from the coupling between the false vacuum and one-bubble states

$$\begin{aligned} \langle G_\Omega \rangle(t) &= \langle \psi(t) | G_\Omega | \psi(t) \rangle, \\ &= \frac{1}{NJ|h_\parallel|} \sum_L \Omega_L \left[\frac{\Omega_L e^{-itE_L}}{E_L} + \frac{\Omega_L e^{itE_L}}{E_L} - 2\frac{\Omega_L}{E_L} \right], \\ &= \frac{1}{NJ|h_\parallel|} \sum_L \frac{\Omega_L^2}{E_L} [e^{-itE_L} + e^{itE_L} - 2], \\ &= \frac{2}{NJ|h_\parallel|} \sum_L \frac{\Omega_L^2}{E_L} [\cos(E_L t) - 1]. \end{aligned} \quad (\text{S71})$$

This term is seen to be intensive and consistent with our initial state as the entire contribution vanishes at $t = 0$.

The second term is related to the magnetization of a bubble state

$$\begin{aligned}
\langle G_\lambda \rangle(t) &= \langle \psi(t) | G_\lambda | \psi(t) \rangle, \\
&= \frac{1}{NJ|h_\parallel|} \sum_{L,L'} \lambda_{L,L'} \frac{\Omega_L \Omega_{L'}}{E_L E_{L'}} \left(e^{i(E_L - E_{L'})t} - e^{-iE_{L'}t} - e^{iE_L t} + 1 \right), \\
&= \frac{1}{2NJ|h_\parallel|} \sum_{L,L'} \lambda_{L,L'} \frac{\Omega_L \Omega_{L'}}{E_L E_{L'}} \left(e^{i(E_L - E_{L'})t} + e^{-i(E_L - E_{L'})t} - e^{-iE_{L'}t} - e^{iE_{L'}t} - e^{iE_L t} - e^{-iE_L t} + 2 \right), \quad (S72) \\
&= \frac{1}{NJ|h_\parallel|} \sum_{L,L'} \lambda_{L,L'} \frac{\Omega_L \Omega_{L'}}{E_L E_{L'}} \left(\cos \{ (E_L - E_{L'})t \} - 2 \cos(E_L t) + 1 \right),
\end{aligned}$$

where in the third line we used the symmetric property of $\lambda_{L,L'}$ seen in Eq. (S42). As for $\langle G_\Omega \rangle$ also $\langle G_\lambda \rangle$ satisfies the consistency check that it vanishes at $t = 0$. One notices that the extensive property of Ω_L is canceled and since $\lambda_{L,L'}$, in Eq. (S42), is intensive the average magnetization is intensive as it should be. After some initial time one expects that the physics is dominated by the resonant bubble. Assuming that an almost resonant bubble exists in the system such that we can expand the cosines the slow envelope of the magnetization grows quadratically

$$\lim_{E_r \rightarrow 0} \langle m_{avg} \rangle(t) = M - \frac{\Omega_r^2 t^2}{NJ|h_\parallel|} (E_R + \lambda_r) = M - \frac{\lambda_r \Omega_r^2 t^2}{NJ|h_\parallel|}. \quad (S73)$$

3. Dynamics of bubbles

The density of bubbles of size n is straight-forward to compute within the single-bubble theory

$$P_n = \frac{1}{N} \left| \langle 0_+ | \sum_m b_m b_{n+m} | \psi(t) \rangle \right|^2 \quad (S74)$$

as the operators b_n action on $|\psi\rangle$ is well-understood. In the many-bubble theory the wave-function has the form

$$|\psi\rangle(t) = \sum_{m,L} c_{m,L} \left(d_L^\dagger \right)^m |0_+\rangle. \quad (S75)$$

The action of b_n on the coherent boson states is highly non-trivial and we can therefore not directly compute P_n . However, if we neglect the quantum cross-terms then we can write an approximation for the overlap between states with fermions a distance n apart and our coherent states given by

$$\langle n | \psi \rangle = \frac{1}{\sqrt{N}} \sum_L \langle d_L^\dagger \rangle \phi_L(n). \quad (S76)$$

Within this approximation P_n is given by

$$\begin{aligned}
P_n &= \frac{1}{N} \sum_{L,L'} \langle d_L^\dagger \rangle \langle d_{L'} \rangle \phi_L(n) \phi_{L'}^*(n), \\
&= \sum_{L,L'} \alpha_{L,L'}(n) \left\{ \cos[t(E_L - E_{L'})] - 2 \cos(tE_L) + 1 \right\}, \quad (S77)
\end{aligned}$$

where

$$\alpha_{L,L'}(n) = \frac{1}{N} \phi_L(n) \phi_{L'}^*(n) \frac{\Omega_L \Omega_{L'}}{E_L E_{L'}}. \quad (S78)$$

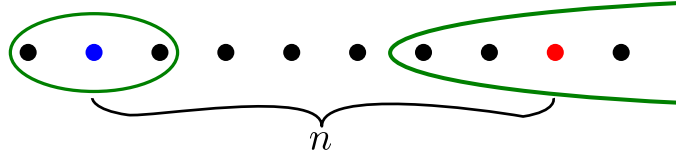


Figure S1. Sketch illustrating how to compute the correlation function. The green ovals represent TV bubbles.

As a sanity check we can compute the total density of bubbles in the system

$$\begin{aligned}
 \sum_n P_n &= \frac{1}{N} \sum_{L,L',n} \langle d_L^\dagger \rangle \langle d_{L'} \rangle \phi_L(n) \phi_{L'}^*(n), \\
 &= \frac{1}{N} \sum_{L,L'} \langle d_L^\dagger \rangle \langle d_{L'} \rangle \delta_{L,L'}, \\
 &= \frac{1}{N} \sum_L \langle d_L^\dagger d_L \rangle, \\
 &= \mathcal{N},
 \end{aligned} \tag{S79}$$

with the excitation density defined in Eq. (S66). So the number-density of spatial bubbles is equivalent to the total number-density of bosonic excitation as one would expect from our simple non-interacting theory.

To show that some care has to be taken with our approximation of P_n we can use it to compute the magnetization. Within our approximate picture and with only a small excitation density, the magnetization should be related to the density of TV domains through

$$m(t) \approx M [1 - 2\rho(t)] = M \left[1 - 2 \sum_n n P_n(t) \right]. \tag{S80}$$

Writing out the last term

$$\begin{aligned}
 -2M \sum_n n P_n(t) &= -2M \sum_{n,L,L'} n \alpha_{L,L'}(n) F(t), \\
 &= -2M \sum_{n,L,L'} \frac{n \phi_L(n) \phi_{L'}^*(n)}{N} \frac{\Omega_L \Omega_{L'}}{E_L E_{L'}} F(t),
 \end{aligned} \tag{S81}$$

where $F(t)$ is the time-dependent function in the curly brackets in Eq. (S77). Writing out the λ -contribution to the magnetization in Eq. (S72) one finds

$$\langle G_\lambda \rangle(t) = \sum_{L,L'} \frac{-2M n \phi_L(n) \phi_{L'}^*(n)}{N} \frac{\Omega_L \Omega_{L'}}{E_L E_{L'}} F(t) = -2M \sum_n n P_n(t). \tag{S82}$$

This means that using P_n to compute the magnetization will be off as the quantum cross-terms from G_Ω in Eq. (S71) are missing. So quantities computed with P_n generically includes additional approximations on top of the ones already present in CBT.

B. spin-spin correlation function

To understand how all spatial structure in the fermions translate into dynamics in the spin chain we consider approximating the spin-spin correlation function given by

$$C_n(t) = \frac{1}{N} \sum_{j=1}^N (\langle \sigma_{n+j}^x \sigma_j^x \rangle - \langle \sigma_j^x \rangle^2). \tag{S83}$$

To approximate this we first want to compute the probability, Q_n , of two spins having opposite magnetization when being separated by n sites. So specifically we want to compute the probability that the red and blue site in Fig. S1 have

opposite magnetization. Consistent with our assumption that the excitation is small we consider the probability in the case when only one bubble is present within this region. There are two different scenarios that must be accounted for. The first is illustrated around the red site in Fig. S1 (ignore bubble around blue site). In this scenario the bubble size l_B is large than the separation between the sites: $l_B > n$. In this case there are n different locations for the bubble such that the red site is covered but the blue site is not. The opposite regime of $l_B < n$ is illustrated around the blue site (ignore the previously discussed bubble around the red site). In this case there are l_B different locations where the blue site is covered and thus gives rise to opposite magnetization of the two colored sites. Putting this together we can write the probability of the two spins having opposite magnetization as

$$Q_n(t) = 2 \sum_l \min(n, l) P_l(t), \quad (\text{S84})$$

where the factor of two arises from the fact that we also have to included the processes where the two sites are swapped (large bubble from the left and small bubble to right). With this object we are able to compute the total spin-spin correlation function as a sum of two contributions. The first is the probability of the two spins pointing in the same direction and the second is the probability of them being opposite

$$\begin{aligned} \mathcal{C}_n(t) &= \frac{1}{N} \sum_{j=1}^N \langle \sigma_{n+j}^x \sigma_j^x \rangle(t), \\ &= M^2 [1 - Q_n(t)] + M^2 [-Q_n(t)], \\ &= M^2 [1 - 2Q_n(t)], \\ &= M^2 \left[1 - 4 \sum_l \min(n, l) P_l(t) \right]. \end{aligned} \quad (\text{S85})$$

To compute the disconnected contribution we consider the limit of $\lim_{n \rightarrow \infty}$

$$\begin{aligned} \lim_{n \rightarrow \infty} \mathcal{C}_n(t) &= \frac{1}{N} \sum_j \langle \sigma_n^x \rangle \langle \sigma_j^x \rangle, \\ &= \frac{1}{N} \sum_j \langle \sigma_j^x \rangle^2, \\ &= M^2 \left[1 - 4 \sum_l l P_l(t) \right], \\ &= M^2 [1 - 4\rho(t)], \end{aligned} \quad (\text{S86})$$

where we have exploited the translation invariance of the system. With these results we can approximate the connected spin-spin correlation function as

$$C_n(t) = 4M^2 \sum_{l=n+1}^N (l - n) P_l(t). \quad (\text{S87})$$

The approximation has the simple intuitive structure that only bubbles larger than the distance between the sites contribute to the connected correlations.

Lastly we remark that for both the magnetization and the correlation function we have neglected the delocalized nature of the domain walls which is only valid if the relevant fermion bubbles are much larger than the domain wall spreading in Eq. (S5). For the considered parameters in the main text this is the case as for the rigid parameters $W_\rho \approx 0.26$ where the resonant bubble is of size 4, while for the expandable regime $W_\chi \approx 3.46$ where the bubbles extend up to more than a hundred lattice sites (see plot of $|\phi_r(n)|^2$ in main text).

[S1] S. B. Rutkevich, Decay of the metastable phase in $d = 1$ and $d = 2$ ising models, Phys. Rev. B **60**, 14525 (1999).

[S2] G. B. Mbeng, A. Russomanno, and G. E. Santoro, The quantum Ising chain for beginners, SciPost Phys. Lect. Notes, 82 (2024).

- [S3] R. Verdel, F. Liu, S. Whitsitt, A. V. Gorshkov, and M. Heyl, Real-time dynamics of string breaking in quantum spin chains, *Phys. Rev. B* **102**, 014308 (2020).
- [S4] G. Lagnese, F. M. Surace, S. Morampudi, and F. Wilczek, Detecting a long lived false vacuum with quantum quenches (2023), arXiv:2308.08340 [cond-mat.stat-mech].
- [S5] As in the case for [S4].
- [S6] M. C. Tichy, P. A. Bouvrie, and K. Mølmer, How bosonic is a pair of fermions?, *Applied Physics B* **117**, 785 (2014).